

Coastal dynamics on equatorial beaches of Amazonian coast during extreme tide events

Leilanne Almeida RANIERI ^{1*}, Renan Peixoto ROSÁRIO ¹, Amanda Sue TRITINGER ² & Maâmar EL-ROBRINI ^{1,3}

¹ Post Graduate Program in Oceanography. Geoscience Institute. Federal University of Pará, Augusto Corrêa Avenue, 1. CEP: 66075-110, Belém, Pará, Brazil (laranieri@ufpa.br ORCID 0000-0002-9870-4879, renanpeixoto@ufpa.br ORCID 0000-0003-2913-0514).

² Engineer Research and Development Center, 3909 Halls Ferry Rd, Vicksburg, MS 39180, USA (atritinger@gmail.com).

³ Post Graduate Program in Naval Engineering. Geoscience Institute. Federal University of Pará, Augusto Corrêa Avenue, 1. CEP: 66075-110, Belém, Pará, Brazil (robrini@ufpa.br ORCID 0000-0001-7850-1217).

Abstract. This paper describes the influence of tidal currents on sediment transport on Amazonian equatorial beaches during extreme tide events. The study area (Salinópolis city) was divided into two sectors: western (Sampaio tidal channel) and eastern (Atalaia Island). Field surveys were conducted in 2013 during two periods of highest tides: April (the rainy season) and October (the less rainy season and Spring Equinox). The optical backscatter sensors (tide, turbidity, and wave data) and current meter sensors (velocity field data) were programmed to collect data every 0.1 and 60 seconds, respectively. They operated together for 24/12 hours on the upper shoreface (surf zone). Wave heights were higher in the Atalaia Island (up to 1.0 meter during the less rainy season). The currents were stronger, reaching 1.2 m.s⁻¹, during ebb tide in the rainy season (Sampaio tidal channel). Higher turbidity values (maximum 1,200 FTU) occurred at the Atalaia Island during the less rainy season. The coastal dynamics in the area derives mostly from the Amazonian continental shelf, where intense tidal currents interact with a high volume of particulate debris, especially fine sand in Salinópolis. Nevertheless, estuaries and tidal channels are also largely responsible for sediment supply and play a key role in shoreline stability and coastal transport, especially during extreme tide events.

Keywords. Salinópolis, Macrotidal, Beach, Tidal Channel, Hydrodynamics.

Resumo. DINÂMICA COSTEIRA EM PRAIAS EQUATORIAIS DA COSTA AMAZÔNICA DURANTE EVENTOS EXTREMOS DE MARÉ. Este artigo descreve a influência das correntes de maré no transporte de sedimentos em praias equatoriais da Amazônia durante eventos extremos. A área de estudo (cidade de Salinópolis) foi dividida em dois setores: oeste (canal de maré do Sampaio) e leste (Ilha do Atalaia). As coletas em campo foram realizadas em 2013 durante dois períodos de marés mais altas: abril (estação chuvosa) e outubro (estação menos chuvosa e equinócio de primavera). Os sensores ópticos de retroespalhamento (marés, turbidez e dados de onda) e sensores de medidor de corrente (dados de campo de velocidade) foram programados para coletar dados a cada 0,1 e 60 segundos, respectivamente. Eles operaram juntos por 24/12 horas na face litorânea superior (zona de surf). A altura das ondas foi maior na Ilha do Atalaia (até 1,0 metro na estação menos chuvosa). As correntes foram mais fortes, atingindo 1,2 m/s, durante a vazante na estação chuvosa (canal de maré do Sampaio). Maiores valores de turbidez (máximo 1.200 FTU) ocorreram na Ilha do Atalaia durante a estação menos chuvosa. A dinâmica costeira na área deriva principalmente da plataforma continental amazônica, onde intensas correntes de maré interagem com um alto volume de detritos particulados, especialmente areia fina em Salinópolis. No entanto, os estuários e canais de maré também são amplamente responsáveis pelo suprimento de sedimentos e desempenham um papel fundamental na estabilidade da costa e no transporte costeiro, especialmente durante eventos extremos de maré.

Palavras-chave. Salinópolis, Macromaré, Praia, Canal de Maré, Hidrodinâmica.

1 Introduction

Coastal zones are dynamic spaces where human activities and infrastructure are exposed to natural forces, climate change, and extreme events (Williams & Lück-Vogel, 2020). They are among the most complex and variable transition systems, as their dynamics are subject to secondary effects of a wide range of hydro-morphodynamic processes, such as winds, waves, tides, and currents, which interact at different spatial and temporal scales (Alvarez-Ellacuria *et al.*, 2010). Beaches protect the coastline environment against the action imposed by the above-mentioned coastal processes, and regulate sediment transport and distribution, resulting in erosion and sediment deposition sectors according to beach dynamics.

The accretion of beaches is supplied by sandy sediment sources derived from the adjacent rivers and inner continental shelf. Substantial littoral transport mechanisms are required for the transfer of material to the beach from these locations or to relocate the material back to the continental shelf (Cartier & Héquette, 2015).

Shore-face deposits are influenced by fair-weather waves, storm waves, and tides. Unlike fair-weather and storm effects on sediment deposition, tidal effects on the character of the shoreface are relatively poorly understood (Dashtgard *et al.*, 2012), especially in meso-macrotidal regions.

Most scientific papers available have focused on subtropical and temperate regions (Almeida *et al.*, 2015; Bosboom *et al.*, 2014; Jamal *et al.*, 2014; Poate *et al.*, 2013, 2014). Few studies have been conducted on meso-macrotidal beaches located in equatorial and/or tropical regions (Sénéchal *et al.*, 2009; Ranieri & El-Robrini, 2012, 2016; Pereira *et al.*, 2013; Oliveira *et al.*, 2014; Nascimento & Pereira, 2016), where beach dynamics have important peculiarities, such as high flow of rivers/estuaries, high intensity of tidal currents, and the presence of moderate wave energy which is modulated by sandy banks/bars.

Tidal current is one of the important forcings in the Amazon coastal zone. It can be defined as the periodic movement of water due

to the pressure gradient force between the crest and trough of the tidal wave. Interaction with bathymetry, margin, and other local aspects affect its characteristics (Owen, 2020). Tidal currents produce a shearing stress on the seabed, which influences sediment transport and grain size distributions (Torres & Uncle, 2021).

Studies on the Amazonian coast are even scarcer, particularly those regarding sediment transport on beaches influenced by macrotides. There are more studies on the subaerial or the emerged area of the beach (swash zone) than on the submerged area of the beach (surf and breaker zones), where methods and techniques for analyzing the littoral process are less defined due to the high turbulence levels generated by breaking waves on the sand bars and strong currents that make it difficult to deploy equipment and collect data. Moreover, when and if data is collected from the coastal zone, a complexity exists in filtering the data due to the entanglement of the physical agents on the fluid.

In contrast, many methods and equipment have been used in other places of the world to study the behavior of sediments in the surf zone. White (1998) highlights methods for measuring coastal sediment transport such as accumulation methods (impoundment), radioactive and fluorescent tracers, traps, optical sensors (which measure sediment concentration in the water column), submerged acoustic sensors for current measurement, and remote sensing through satellite images, aerial photographic images, and radars. These methods have been adapted for longshore transport studies in subtropical and temperate regions, but this is not the case for the Amazonian equatorial beaches.

Among the methods listed, optical and acoustic sensors have been increasingly deployed in coastal/marine environments to study coastal processes due to their high frequency of data collection and thus their ability to observe orbital wave velocities and sediment concentration (Osborne & Greenwood, 1993; Aagaard & Greenwood, 1995; Vincent & Osborne, 1995; Beach & Sternberg, 1996; Voulgaris & Collins, 2000; Cartier & Héquette, 2015).

On the Salinópolis coast the tides have a strong influence on sedimentary transport

(Pereira *et al.*, 2014). Its main beaches are Corvina, Maçarico, Farol Velho and Atalaia (Fig. 1). Between Maçarico and Farol Velho beaches is the Sampaio tidal channel, which has an important role in the local sedimentary dynamics (Ranieri & El-Robrini, 2015). The Corvina and Atalaia beaches are limited by tidal-dominated estuaries. This means that the tidal currents on these beaches can have an effect on the intensity or direction of other physical processes (waves, currents generated by waves, and turbidity), and consequently, they govern sedimentary dynamics.

This paper describes the influence of tidal currents on sediment transport on Salinópolis macrotidal beaches during extreme events. The objective is to collect and analyze velocity field, tide, turbidity, and wave data obtained from two surveys at Salinópolis city (Oriental Amazon), using optical and magnetic sensors.

2 Study area

This study was conducted at four sandy macrotidal beaches in Salinópolis city (Fig. 1). According to Aguilera *et al.* (2020), the stratigraphic location of beaches seems to be at the very top of the entire Pirabas Formation (sedimentary carbonate rocks), just below the contact with the overlying Barreiras Formation (fully siliciclastic unit), evident on cliffs in the region. On these units, stratigraphic are the sedimentary deposits of the Post-Barreiras and recent Quaternary. These sediments are associated with tidal influence, characterizing the current plains of rivers, mangroves, and beaches (Sá, 1969). On the latter, there is a predominance of fine sands, with moderately to poorly selected medium grain-size in isolated points of the beaches, close to the rocky outcrops of the Pirabas Formation (Ranieri & El-Robrini, 2020).

Beaches on the Amazonian coast are dominated by tidal currents, which play an important role in local circulation. They strongly influence coastal sediment transport (Souza Filho & Paradella, 2003). The maximum velocity of the tidal currents on the inner continental shelf of Northern Brazil during spring tide is $2 \text{ m}\cdot\text{s}^{-1}$ (Cavalcante *et al.*, 2013).

Wind, wave, and current dynamics in this region are primarily regulated by the weather (equatorial climate). Local wave and current patterns are also shaped by the physical and sedimentary structure of large estuaries that flow into the Amazonian coast (for example, the Amazon, Pará, Marapanim, Maracanã, Arapepó, Caeté, and Emboraí Rivers). Another key physical forcing factor is the semidiurnal tide that can reach up to 5 meters in amplitude during high spring tides (Prestes *et al.*, 2017).

Oceanographic conditions are largely influenced by the natural annual weather variability (the rainier and the less rainy seasons) in the Amazonian coast. Beyond this there are El Niño/Lã Niña oscillations that occur in the Pacific and Atlantic oceans. These two major sea surface temperature irregularities influence the variability of interannual Amazonian rainfall, and as a result are known to generate the Atlantic dipole phenomenon known, a to alter the Sea Surface Temperature (SST) anomaly pattern (Bulgin *et al.*, 2020). This in turn influences the intensity and position of the Intertropical Convergence Zone (ITCZ), whose average position changes seasonally from 9° N to 2° N on the Equatorial Atlantic Ocean (Utida *et al.*, 2019). The migration of the ITCZ in the equatorial Atlantic Ocean has a large effect on the annual rainfall cycle in the region of interest.

As the ITCZ migrates towards the northern hemisphere, winter and spring will observe a less rainy season. Therefore, when a storm does occur, it is an isolated, quick event with heavy rainfall, and high-magnitude accompanying wind speeds. In the region of Salinópolis, the volume of rainfall is lower in the months of September, October, and November. The rainy season starts in December and lasts five to six months. The wettest period (March-April-May) is caused by the intensification of local effects associated with the presence of the ITCZ, which is closer to the Southern Hemisphere during this period (Albuquerque *et al.*, 2010). According to the historical series, the annual rainfall in Salinópolis is approximately 2.800 mm (ANA, 2013).

The dominant wind regime is represented by Northeast (NE) trade winds which operate continuously throughout the year. These are

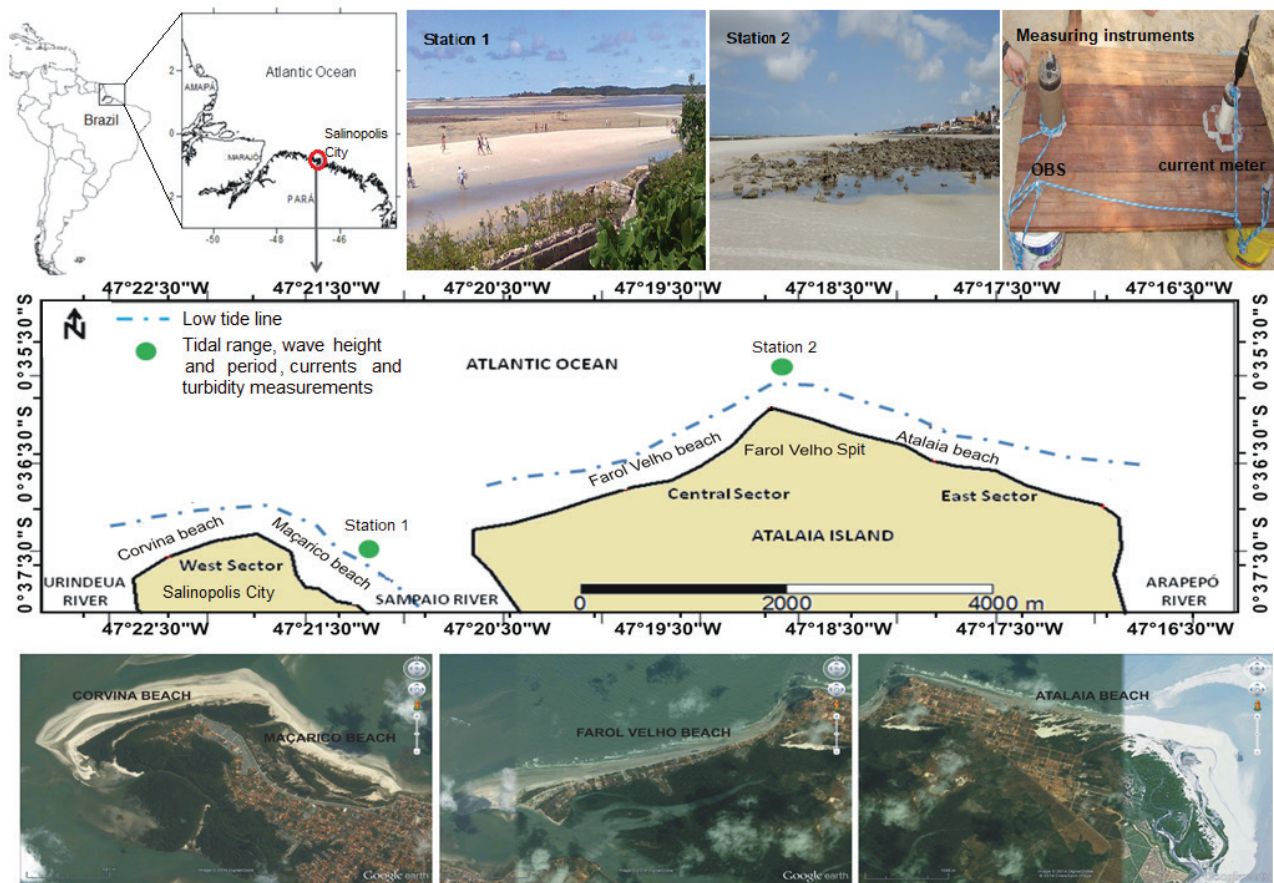


Figure 1. Map of the study area with data collection stations (green dots) (Spot 5 satellite images captured on 10/19/2009, available at Google Earth).

Figura 1. Mapa da área de estudo com as estações de coleta de dados (pontos verdes) (Imagem do satélite Spot 5 capturada em 19/10/2009, extraído do Google Earth).

responsible for sediment transport from the inner continental shelf towards the coast (Geyer *et al.*, 1996). The average wind speed of the NE trade winds was $4.1 \text{ m}\cdot\text{s}^{-1}$, and the change in direction was predominantly $20\text{--}30^\circ$ (Fig. 2) (CPTEC, 2014) for the year 2013 in Salinópolis city.

These prevailing winds form waves and cause longshore currents to flow northwestward (Geyer *et al.*, 1996). According to CPTEC (2013), forecast with the WAVEWATCH (WW) model, wave height in Salinópolis ranges from 0.5 to 1.5 m.

The tides in the Salinópolis area are semidiurnal and reach maximum heights of approximately 6.0 meters (macrotides). According to one and a half years of tidal observations from the Brazilian Navy – Directorate of Hydrography and Navigation (DHN, 1962 and Carvalho, 2007), at the Salinópolis station, water level values were as follows: the spring tidal range was on average 4.82 meters and the neap tidal range was on

average 2.64 meters. From this monitoring, the highest ebb (January) and flood (June) currents observed reached about $1.44 \text{ m}\cdot\text{s}^{-1}$ and $1.13 \text{ m}\cdot\text{s}^{-1}$, respectively.

The main beaches in Salinópolis (Corvina, Maçarico, Farol Velho, and Atalaia) are exposed to the Atlantic Ocean (Fig. 1). The sediment classification of these beaches is predominantly made up of fine, well-selected sand, with a dissipative morphodynamic state that is exposed to high-energy conditions by waves and tides (Ranieri & El-Robrini, 2015).

3 Materials and methods

3.1 Data Acquisition

The study area was divided into two regions; Salinópolis city and its main island: Atalaia Island (shown in Fig. 1). The first beach segment (Corvina and Maçarico) is in Salinópolis

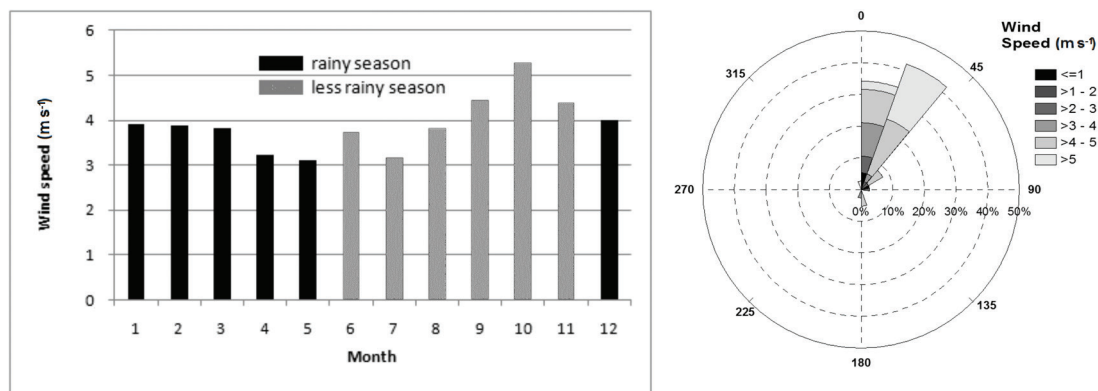


Figure 2. Average wind speed and direction in the Salinópolis coast in 2013 (CPTEC, 2014).
 Figura 2. Direção e velocidade média dos ventos na costa de Salinópolis em 2013 (CPTEC, 2014).

(western sector), and the second segment (Farol Velho and Atalaia) is in Atalaia Island (eastern sector).

Field surveys were conducted in 2013 during two period of the highest tides: April 26-28 (the rainy season) and October 4-6 (the less rainy season and the Spring Equinox). During these periods, currents, turbidity, tidal height, wave period, and wave height were measured in multiple locations. One location was on Maçarico beach (western sector), so chosen due to the high influence of the Sampaio tidal channel on sediment transport there. The other location was on Atalaia Island (eastern sector), which was chosen because of an area along the coast, known as Farol Velho Spit (Fig. 1), that has the most turbulent and exposed coastline. Here refraction of waves causes bidirectional longshore currents that are important for sediment transport in the area.

Data on turbidity, tidal height, wave period, and wave height were obtained using the Optical Backscatter Sensors (OBS) Infinity-turbi ATU75W-USB model. Data on currents were recorded with a magnetic Current Meter Infinity AEM-USB model. The OBS and Current Meter sensors were programmed to collect data every 0.1 and 60 seconds, respectively. Thus it was even possible to analyze the water level variations caused by waves, allowing the processing and filtering of wave height and period data in the MatLab 8.5 software.

The pieces of equipment operated together for 12.3 hours (1 spring tidal cycle) starting at

the turn of Low High Water (LHW) on the upper shoreface (surf zone). Except at Farol Velho Spit during the rainy season, the equipment measured the data for up to 25 hours. In this case, the aim was to represent better the data for this season, where it is expected that there will be a more significant discharge from the channels. Complementary data from forecasting models and measurement instruments available on virtual platforms of government research institutions were also used to determine the meteorological and oceanographic status of the region during the months of collection, such as the WW model for wave prediction and the Synop Station for wind data.

3.2 Data process

The time series of the velocity field (intensity and direction) was converted into longitudinal (u) and transversal components (v). Where v is the current intensity and θ is the trigonometric angle formed between the abscissa (Ox), measured in an anti-clockwise rotation. The orientation of data represented in this study reference a northward facing velocity field, where positive values of the velocity component v and negative values of the velocity component u represent ebb tide. The reverse, v (-) and u (+), represent flood tide. The velocity field decomposition theory applied in this study is shown in greater detail in De Miranda *et al.* (2017).

The significant wave height (H_s) was calculated according to methods similar to that

of Holthuijsen (2007). Spectral analysis was performed to isolate the frequency bands from the time series (Emery and Thomson, 2014). The wave height (H) is the vertical distance between the highest and the lowest surface elevation in a wave. To obtain the characteristic of the wave " H_s " was calculated based on equation 1:

$$H_s = \frac{1}{N/3} \sum_{j=1}^{N/3} H_j \quad \text{Eq. (1)}$$

Where " N " is the total number of wave height records and " j " represents the rank number of the wave, based on wave height (i.e., $j = 1$ is the highest wave, $j = 2$ is the second-highest wave, etc).

The spectral analysis used in this work was based on the method proposed in Welch (1967) with a Hanning window with 50 % overlap, and that was 1/3 (one third) of the total length of the time series. Thus, the estimate of average spectral density is calculated from the estimate of five segments. The " Y " axis of the power spectral density was normalized ($NPSD$) for better visualization of the results according to equation $NPSD = PSD / \max(PSD)$.

4 Results

The significant wave height in the Sampaio tidal channel in April and October never exceeded 12 and 10 centimeters, respectively. These values were the maximum wave heights observed and occurred during the high tide period (Fig. 3A, 4A). The highest turbidity values occurred during flood tide in April (the rainy season) (Fig. 3B), and during ebb tide in October (Spring Equinox and the less rainy season) (Fig. 4B).

The local current at the sample points is essentially tidally driven, which means well-defined flood and ebb tidal current. The velocity vectors showed greater intensity during the ebb in the Sampaio tidal channel that reached instantaneous values up to $1.2 \text{ m}\cdot\text{s}^{-1}$ in April (Fig. 3C). At this point, the Sampaio tidal channel location, the " v " component (the cross-shore current - gray line in Fig. 3C) is more significant in water movement than the " u " component (the longshore current - black line in figure 3C).

The April event (the rainy season and spring tide) recorded a tide of approximately 5.4 meters on the Sampaio tidal channel (western sector) (Fig. 3D). The tidal asymmetry was positive. This asymmetry was more significant in the tidal channel, due is more sheltered. At this point, the flood period was approximately 4 hours and the ebb was approximately 7 hours during the October event (the less rainy season and Spring Equinox). The tidal behavior during this event was similar, where the tidal channel and Atalaia Island (eastern sector) reached 5.4 meters as well and exhibited positive asymmetry (Fig. 4D, 4H).

Already the maximum significant wave height reached 1.1 meters on Atalaia Island and occurred during high tide in April (Fig. 3E). In October, this maximum was 0.6 meters and occurred at the end of the flood tide (Fig. 4E). The highest turbidity values occurred during ebb tide (Fig. 3F, 4F).

The longshore (u) and cross-shore (v) currents showed similar intensities. Most notably, the highest value of the " u " component was during the flood tide period, which was $0.7 \text{ m}\cdot\text{s}^{-1}$ (Fig. 3G, 4G). In April event (the rainy season and spring tide), a tide was approximately 4.0 meters (Fig. 3H), with positive asymmetry in the Atalaia Island.

The power spectral density estimates of the wave time series in the Sampaio tidal channel showed dominant frequency bands with periods of 9.8 and 50 seconds in April (Fig. 5A), and periods of 6, 12, and 50 seconds in October (Fig. 5B). For the time series of the Atalaia Island the dominant periods were 20 and 9.0 seconds in April (Fig. 5C) and 12 and 6 seconds in October (Fig. 5D).

5 Discussion

5.1 Hydrodynamic

The tide range was 4.0 meters at Atalaia Island, during the rainy season, to 5.4 meters at Atalaia Island and Sampaio tidal channel, during the less rainy season (Fig. 3). The highest tidal levels observed were due to the equinoctial tide (Spring Equinox) (Fig. 2). The lowest tidal level recorded occurred when the Autumn Equinox

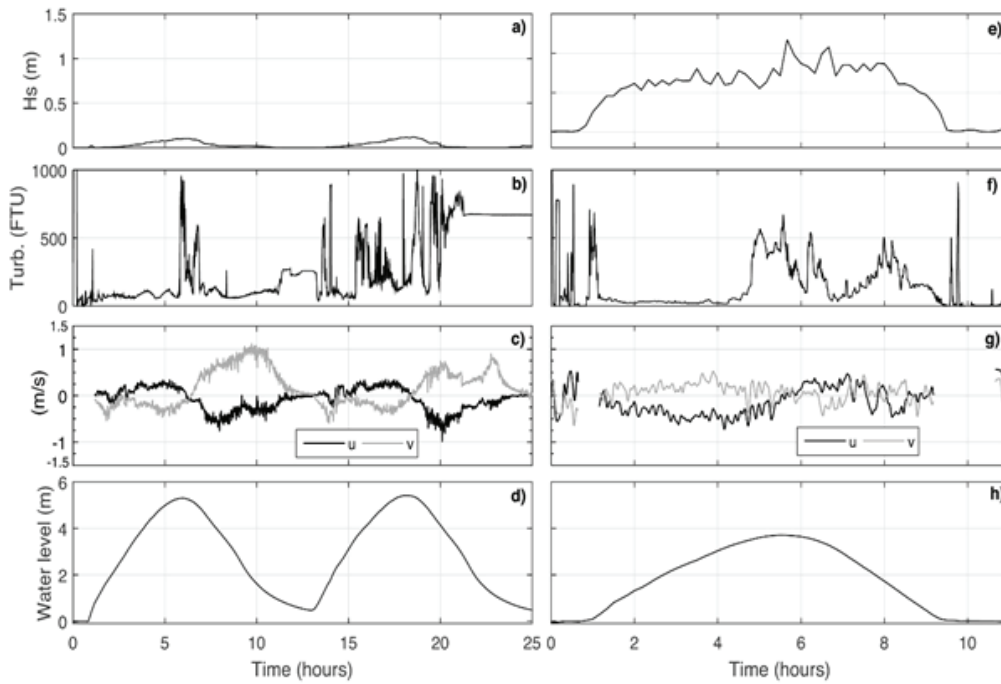


Figure 3. Time series of significant wave height (H_s , meters), turbidity (FTU), velocity components u (black, $m \cdot s^{-1}$) and v (gray, $m \cdot s^{-1}$), and water level (meters) during the April field experiment. On the left (A), (B), (C), and (D): the Sampaio tidal channel. On the right (E), (F), (G), and (H): the Atalaia Island. The positive values of " v " and negative values of " u " represent ebb. In contrast, when " v " is negative and " u " is positive, it represents a flood.

Figura 3. Séries temporais de altura de onda significativa (H_s , metros), turbidez (FTU), componentes de velocidade u (preto, m/s) e v (cinza, m/s), e nível de água (metros) durante o experimento de campo de abril. À esquerda (A), (B), (C) e (D): canal de maré do Sampaio. À direita (E), (F), (G) e (H): Ilha da Atalaia. Os valores positivos de " v " e os valores negativos de " u " representam vazante. Em contraste, quando " v " é negativo e " u " é positivo, representa a enchente.

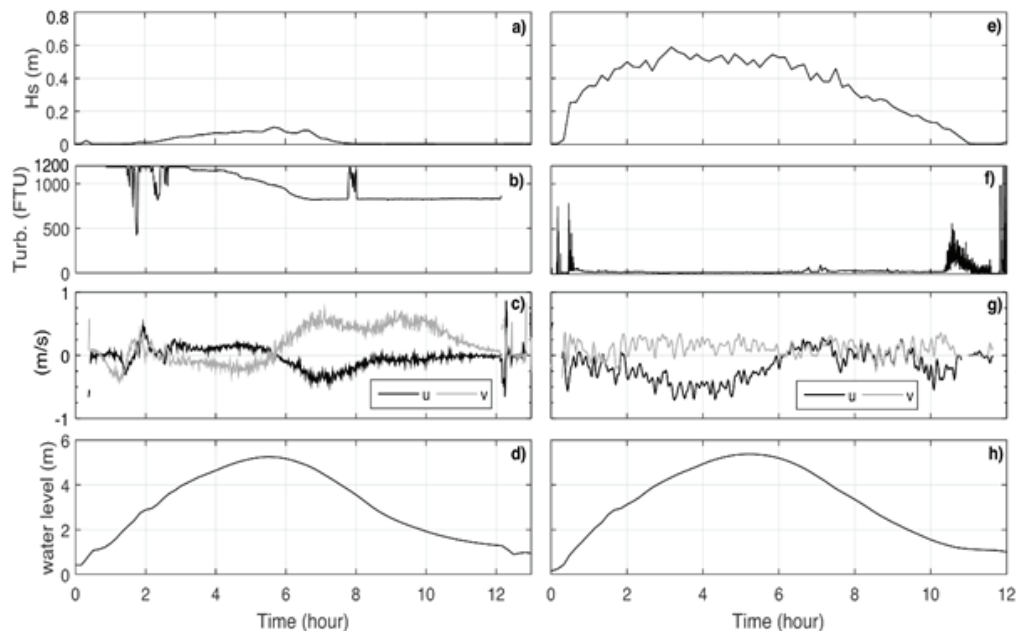


Figure 4. Time series of significant wave height (H_s , meters), turbidity (FTU), velocity components u (black, $m \cdot s^{-1}$) and v (gray, $m \cdot s^{-1}$), and water level (meters) during the October field experiment. On the left (A), (B), (C), and (D): the Sampaio tidal channel. On the right (E), (F), (G), and (H): the Atalaia Island. The positive values of " v " and negative values of " u " represent ebb. In contrast, when " v " is negative and " u " is positive, it represents a flood.

Figura 4. Séries temporais de altura de onda significativa (H_s , metros), turbidez (FTU), componentes de velocidade u (preto, m/s) e v (cinza, m/s), e nível de água (metros) durante o experimento de campo de outubro. À esquerda (A), (B), (C) e (D): canal de maré do Sampaio. À direita (E), (F), (G) e (H): Ilha da Atalaia. Os valores positivos de " v " e os valores negativos de " u " representam vazante. Em contraste, quando " v " é negativo e " u " é positivo, representa a enchente.

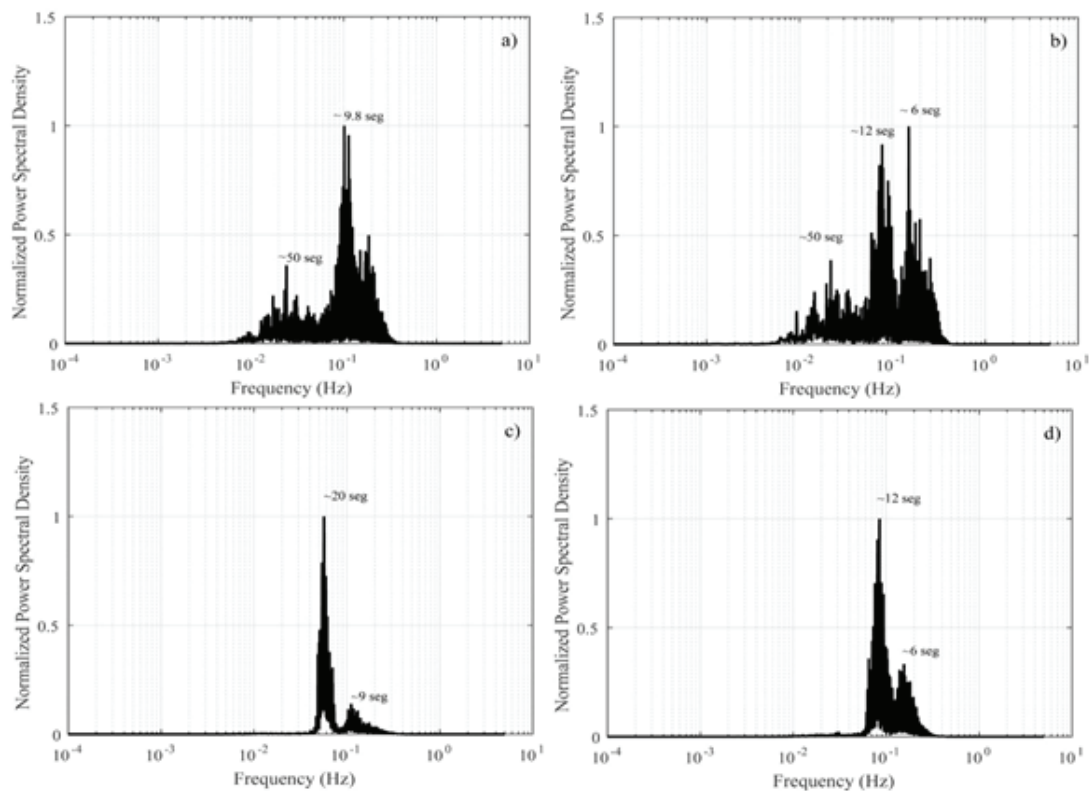


Figure 5. Normalized Power spectral density (NPSD) of wave signals. Frequency in hertz (Hz); spectra are in units of power/Hz. (A) and (B) are NPSD for the Sampaio tidal channel in April and October, respectively. (C) and (D) are NPSD from Atalaia Island in April and October, respectively.

Figura 5. Densidade espectral de potência normalizada (NPSD) de sinais de onda. Frequência em hertz (Hz); os espectros estão em unidades de potência/Hz. (A) e (B) são NPSD para o canal de maré do Sampaio em abril e outubro, respectivamente. (C) e (D) são NPSD da Ilha de Atalaia em abril e outubro, respectivamente.

influence was minimum (data collection about a month after the event). The equinoctial tide events in the region generate tidal ranges up to 5.5 m in Ajuruteua beach about 80 km eastward of Salinópolis (Oliveira *et al.*, 2014) and 5.8 m in Algodoal Island about 24 km westward of Salinópolis (Pereira *et al.*, 2012).

Findings show that the tides are semidiurnal, with slight asymmetry, due to the flood period occurring at a shorter time interval than the ebb period. Tidal asymmetry has been intensively studied because of its controlling role on residual sediment transport and large scale morphological evolution (Guo *et al.*, 2019).

Sandbars (or bars) protect the beach from wave action during part of the ebb tide, high, and low tide, frequently occur along the Amazon's coastline. The result inside these coastal areas is longer ebb tide periods, especially during Equinox.

On beaches with higher open sea exposure, the tidal asymmetry is small due to the low influence of the sandbar, as noted in this article (Pereira *et al.*, 2014).

These features are also seen in other beaches with high sandbar presence, especially in macrotidal coasts. Cartier & Héquette (2015), for example, show that several sandbanks present in the infratidal zone and inner continental shelf, as well as the gentle beach slopes that characterize the northern coast of France, are responsible for strong wave power dissipation. During high tide, the waves can propagate without breaking the bars, and the energy dissipation is faster. Infragravity waves may prevail during these conditions as well.

The infragravity wave band appears to contain some importance in the Sampaio tidal channel. Infragravity waves are present in the time

series in both the months of April and November (Fig 5A, 5B). The Atalaia beach (more exposed to the sea) is dominated by sea and swell waves (Fig. 5C, 5D). Aagaard *et al.* (2013) collected hydrodynamic measurements on a sandy bar at the surf zone of Skallingen, a highly dissipative beach (SW Denmark, North Sea), where it was observed that wind waves, often swell, gradually decreased, while low-frequency waves energy gradually increased, as infragravity energy was dominant. The dominant sea and swell waves in the most exposed regions favor the appearance of the infragravity waves in the Sampaio tidal channel (most sheltered).

During this research, it was observed that the “*Hs*” parameter is associated with tidal phase. “*Hs*” reached the highest values in the Atalaia Island, and always at flood tide (Fig. 3B, 4B). A study, Cartier & Héquette (2015), was conducted in northern France at macrotidal beaches during higher power conditions. During this study, the highest wave heights were recorded when it was close to high tide, while the lowest wave heights were recorded during ebb tide or early flood. Other studies conducted at France's northern beaches showed similar characteristics to Amazon macrotidal beaches, even under storm wave conditions (Sipka & Anthony, 1999; Voulgaris *et al.*, 1998; Levoy *et al.*, 2000; Masselink & Anthony, 2001; Anthony *et al.*, 2004; Reichmüth & Anthony, 2008).

On the Salinópolis beaches longshore currents are also influenced by tidal effect, with directional variability regulated by the ebb and flood tides of the estuaries and tidal channel. Ranieri & El-Robrini (2012) and Oliveira *et al.* (2014) had similar findings, thus attributing peculiarities which are restricted to the Amazonian coast, as the influence of macrotides and large estuarine systems in this study region outweighs the effect of oceanographic patterns found in most coastal zones in Brazil and worldwide.

Brand *et al.* (2020) observed that during spring tide on Belgian macrotidal beaches the alongshore oriented tide-generated currents dominate.

On the northern macrotidal beaches of France, Cartier & Héquette (2015) also had similar findings, with longshore currents essentially

forced by tides under low-energy wave conditions, and observed the flood and ebb tidal currents flowing in opposite directions. However, the coast of Salinópolis also is influenced by high-energy waves on the Atalaia Island (Fig. 3E, 4E), which contribute to lower bidirecting the longshore current. In Atalaia Island, currents directed towards the Sampaio channel (SW direction) occur during ebb tide due to the incidence of NE waves. In other words, currents generated by waves flow in the opposite direction of currents originating from the ebb tide in the Sampaio channel. The predominance of currents was southwestward, and the “*u*” component was found to be negative, and the longshore current direction (Fig. 3G, 4G) was preferentially the same during flood tide. Therefore, in Atalaia Island, longshore currents (*u* component) are bidirectional during ebb tide and are directed preferentially westward throughout flood tide.

Ranieri & El-Robrini (2016) also recorded this occurrence on Atalaia Island, with the influence of the wave incidence, generating currents frequently in the Southwestern (SW) direction in the western part of the Island (central sector of Salinópolis). This occurred during flood tide, and even during ebb tide whose wave incidence angle varied from 5° to 20° NE in April/2013, and 15° to 45° NE in October/2013 (Fig. 6; Fig. 7). In the eastern part of the island, they were able to more clearly observe the bi-directionality of the currents due to the tide. This was also observed in the western sector of the Salinópolis coast, which was greatly influenced by the Sampaio tidal channel. They explained that this behavior of coastal hydrodynamics resulted in a pattern of sediment transport that favors erosion at Farol Velho Spit, and the deposition of sediment at the ends of Atalaia Island. But mainly for the western sector of Salinópolis.

They found that the longshore sediment transport rate (*Qs*) obtained with portable traps during an extreme tide of the rainy season was highest during flood tide (Fig. 6). During the extreme tides of the less rainy season, longshore transport was higher throughout the ebb tide (Fig. 7) when tidal currents joined the higher effect of wave-generated currents, reaching the coast predominantly in the NE direction.

Stronger winds in October increased sediment remobilization by the waves. In this condition, the minimum sediment transport rate was 20 kg.m^{-3} (west sector of Salinópolis) and the maximum was 79 kg.m^{-3} (eastern part of Atalaia Island) (Fig. 7). In April (Fig. 6), a minimum of 2 kg.m^{-3} (west sector of Salinópolis) and a maximum of 32 kg.m^{-3} (western part of Atalaia Island) transport rates were observed. Additionally, it was recorded through the textural observation of the collected sediments that there was a greater occurrence of fine grain-size in suspension. These authors concluded that the lower longshore sediment transport rate obtained in the western sector indicates decreased transport and a sediment deposition zone.

The cross-shore currents as well as their influence on onshore-offshore sedimentary transport were analyzed. The "v," cross-shore, component in Atalaia Island was highly variable in direction, especially in the extreme tidal events during the rainy season (Fig. 4G), where the

vectors northward (onshore-offshore transport) were as frequent as those southward (offshore-onshore transport). It is suggested that the sediment input into the beach system of the Atalaia Island, although low, is due to a higher occurrence of southward current vectors, which highlights the important role of the continental shelf as a sediment source to the coastal zone of Salinópolis. However, features that are unstable to Atalaia Island due to the high frequency of currents flowing towards the continental shelf are also significant. The central sector lacks sedimentary environments on the shoreline in nearly its entire extension due to anthropogenic activities (urbanization). The presence of these environments could help offset the loss caused by the removal of beach sediments by cross transport.

According to Aagaard *et al.* (2013), for a given measurement location, liquid infragravitational flows are often directed towards the continent during low tide and towards the ocean during high

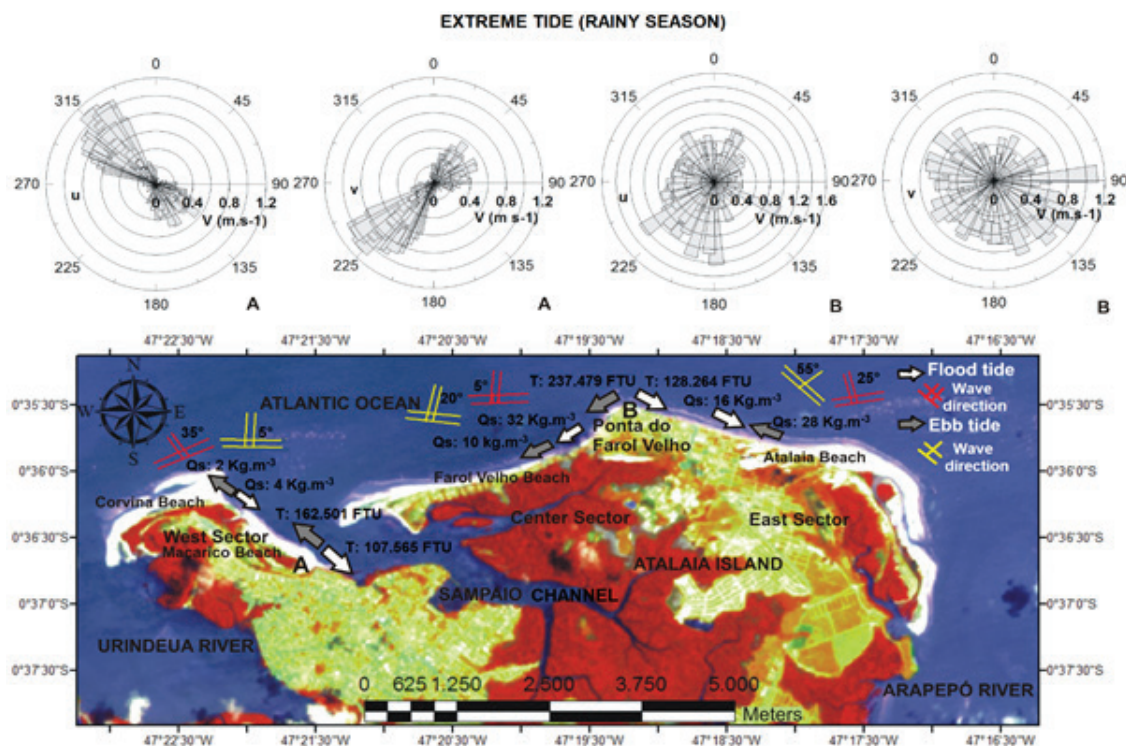


Figure 6. Velocity (m.s^{-1}) and direction (0-360 degrees) of the longshore (u component) and cross-shore (v component) currents, obtained at the Sampaio tidal channel (A) and the Ponta do Farol Velho (Atalaia Island) (B) on April 26-28, 2013. Arrows indicate the preferred direction of the longshore currents during the flood and ebb tides in the beaches. T: turbidity (average value). Qs: longshore sediment transport rate (obtained from Ranieri & El-Robrini, 2016).

Figura 6. Velocidade (m/s) e direção (0-360 graus) das correntes longitudinais (componente u) e transversais (componente v), obtidas no canal de maré do Sampaio (A) e na Ponta do Farol Velho (Ilha de Atalaia) (B) em 26-28 de abril de 2013. As setas indicam a direção preferencial das correntes litorâneas durante as marés de enchente e vazante nas praias. T: turbidez (valor médio). Qs: taxa de transporte de sedimentos litorâneos (obtido de Ranieri & El-Robrini, 2016).

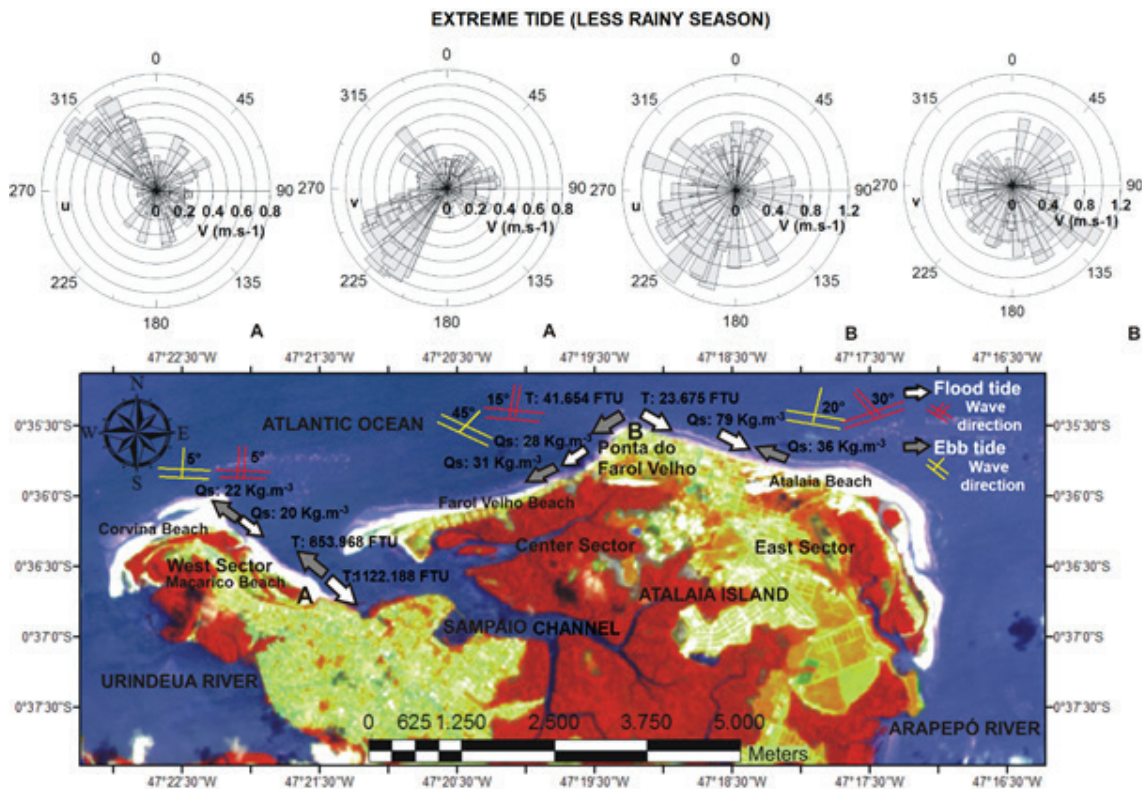


Figure 7. Velocity ($m \cdot s^{-1}$) and direction (0-360 degrees) of the longshore (u component) and cross-shore (v component) currents, obtained at the Sampaio tidal channel (A) and the Ponta do Farol Velho (Atalaia Island) (B) on October 4-6, 2013. Arrows indicate the preferred direction of the longshore currents during the flood and ebb tides in the beaches. T: turbidity (average value). Qs: longshore sediment transport rate (obtained from Ranieri & El-Robrini, 2016).
 Figura 7. Velocidade (m/s) e direção (0-360 graus) das correntes longitudinais (componente u) e transversais (componente v), obtidas no canal de maré do Sampaio (A) e na Ponta do Farol Velho (Ilha de Atalaia) (B) em 4-6 de outubro de 2013. As setas indicam a direção preferencial das correntes litorâneas durante as marés de enchente e vazante nas praias. T: turbidez (valor médio). Qs: taxa de transporte de sedimentos litorâneos (obtido de Ranieri & El-Robrini, 2016).

tide, which can be associated with transverse displacement at a maximum energy dissipation location. At the Sampaio tidal channel longshore currents were quite strong, reaching velocity of $1.2 m \cdot s^{-1}$ on 04/26/2013 during the extreme tide of the rainy season (Fig. 3). Both in this event and in equinoctial tide of the less rainy season (10/04/2013), the highest current velocities were observed during ebb tide, and this was a major hydrodynamic factor at that site. Nevertheless, at Atalaia Island the current velocity had low variability between ebb and flood tides during the two events (Fig. 4). The longshore current velocities at Atalaia Island during these two time periods were mostly between 0.4 and $0.7 m \cdot s^{-1}$. Both the wave energy and tides are responsible for the intensity of currents on the island.

At the Sampaio tidal channel, residual vectors of longshore and cross-shore currents showed a transport pattern both during the extreme tidal events of the rainy season and

Spring Equinox, with bidirectional currents (Fig. 3), and a similar velocity observed at both transport components. However, much stronger currents directed towards the ocean were recorded for the longshore component (u) indicating that it acts as a sediment exporter to the adjacent beaches (Maçarico and Corvina). For the cross-shore component (v) there is also a tendency to export sediments due to the higher frequency of stronger currents southwestward. This is in agreement with the findings of Ranieri & El-Robrini (2015), which indicate a depositional trend during a long period in the western sector, providing coastal progradation; the shoreline average advancement between 1988 and 2013 was 270 meters. According to Souza Filho & Paradella (2003) the entire coast of Maranhão and Pará (Brazil) is rapidly prograding mostly due to the large supply of fine sediments of the numerous estuaries.

5.2. Turbidity

Turbidity on Sampaio tidal channel was high. On the left bank of the channel during the less rainy season, turbidity was much higher (equinoctial tide event), with values during flood tide (average of 1,122 FTU) higher than those during ebb tide (average of 853 FTU) (Fig. 3; Fig. 7). This is likely because the tidal wave penetrates more effectively into the channel the strong tidal currents allow the remobilization of a more significant amount of material (Siegle *et al.*, 2009).

Residence time of suspended material and current intensity are also important factors. According to Kjerfve (1989), the average vector of currents has a serious implication on the residence time of materials present in estuaries. Weaker currents occurred during the less rainy season, increasing the availability of suspended material. In addition, NE winds were stronger in October, 2013, with records of $5.0 \text{ m}\cdot\text{s}^{-1}$ (CPTEC, 2014), causing increased mixture in the water column. River discharge reach into the ocean is also lower during this period, and the availability of suspended particulate matter on Maçarico beach is more conducive. During the rainy season, this availability of suspended material is higher in the stretch of the outer beaches, which receive sediment loads coming from the channel.

When currents are stronger during the rainy season, higher speeds cause higher grain-size variability in the water column in both flood and ebb tides, thus this is when maximum values of sediment mobility occur. The highest contribution of particulate matter coming from the river during ebb tide has provided this tidal phase with higher turbidity during the extreme tide event of the rainy season (approximately 1,000 FTU), but no greater than turbidity during the less rainy season.

On Atalaia Island, higher turbidity values also occurred during this event and ebb tide. The island is a place of high refraction and wave energy dissipation. Wave breaking is widely recognized as inducing large-scale turbulence which is responsible for increasing bed sediment remobilization and suspended sediment concentration (Yu *et al.*, 1993; Beach &

Sternberg, 1996; Voulgaris & Collins, 2000; Ogton & Sternberg, 2002; Cartier & Héquette, 2015).

Because of the association of wind-generated wave energy, tidal waves, the higher effect of tidal currents, as well as the sediment load coming from estuaries during the extreme tide of the rainy season, higher levels of turbidity were found at Atalaia Island during this event (Fig. 4; Fig. 6), which is likely mobilizing finer particulate matter.

6 Conclusions

The extreme tidally driven processes outlined above occur on beaches of the Amazonian coast mainly, during periods of equinoctial tides. Usually, the time of the ebb tide lasts longer than the time of flood tide during a single tidal cycle, indicating positive asymmetry.

Longshore currents on Amazonian beaches are influenced by large estuarine systems that flow into the coast and by the tidal forcings. It is worth noting that, over a long stretch of beach, the longshore current direction can be regulated by flood and ebb current directions of estuaries and tidal channels flowing along the coast. Beaches can also be highly accreted by large estuarine sediment input.

Hydrodynamics on the Amazonian coast change seasonally, i.e., during the rainy and the less rainy seasons. During the rainy season, when there is an increase in the river discharge, and the ebb and flood currents are stronger, tidal currents dominate the beach sedimentation processes. However, during the less rainy season, when winds are stronger, longitudinal currents generated by waves can have a more intense effect on these processes, with enhanced NE-SW longitudinal sediment transport, allowing more significant sediment transfer from one sector (central) to the other (west).

Significant wave height (H_s) was found to be associated with the tidal phase. The highest values were observed during flood tide at Atalaia Island, the region most exposed to the open sea.

Based on the analysis of longshore and cross-shore currents at Farol Velho Spit, Atalaia Island (eastern sector), and at the mouth of the

Sampaio tidal channel, which separates the island from the western sector, it was possible to investigate whether there are important sedimentary exchanges between these two regions, which comprise the oceanic coast of Salinópolis, as well as to examine the influence of the Sampaio tidal channel on sediment transport.

In Salinópolis, considering the current direction and velocity during two extreme tide events in 2013, first in the rainy season (April 26-28) and second in the Spring Equinox (October 4-6, the less rainy season), positive sediment transport was observed towards the strip of beaches in the western sector. At the center of Atalaia Island, longshore currents shifted westwards and intense ebb currents of the Sampaio tidal channel also flowed westwards. The cross-shore currents in this channel also indicated sediment transported to Maçarico beach (western sector).

It is concluded that the coastal dynamics in the area derive mostly from the Amazonian continental shelf, where intense tidal currents interact with a high volume of particulate debris, especially fine sand. Nevertheless, estuaries and tidal channels are also largely responsible for sediment supply and play a key role in shoreline stability and coastal transport, especially during extreme tide events.

The large number of estuaries on the Amazonian coast creates positive conditions of sediment accretion. In the presence of a high discharge rate of river sediments into a coastal region due to strong tidal currents, this coast can become locally progradational.

Acknowledgements. We are grateful to the members of the Marine and Coastal Studies Group (GEMC) of the Federal University of Pará (UFPA) for our partnership in this study. We also thank the Foundation for Support and Development of Research (FADESP), and the Foundation for Research Support of the Pará State (FAPESPA) for granting the scholarship. The Post-Graduate Program in Geology and Geochemistry (PPGG) of UFPA, and the Pro-Rector of Research and Post-Graduate studies (PROPESP/UFPA).

References

- Aagaard, T. & Greenwood, B. 1995. Suspended sediment transport and morphological response on a dissipative beach. *Continental Shelf Research*, 31: 1061-1086.
- Aagaard, T., Greenwood, B. & Hughes, M. 2013. Sediment transport on dissipative, intermediate and reflective beaches. *Earth-Science Review*, 124: 32-50.
- Aguilera, O., Araújo, O.M.O., Hendy, A., Nogueira, A.A., Nogueira, A.C., Maurity, C.W., Kutter, V.T., Martins, M.V.A., Coletii, G., Dias, B.B., Silva-Caminha, S.A., Jaramillo, C., Bencomo, K. & Lopes, R.T. 2020. Palaeontological framework from Pirabas Formation (North Brazil) used as potential model for equatorial carbonate platform. *Marine Micropaleontology*, 154: 101813.
- Albuquerque, M.F., Souza, E.B., Oliveira, M.C.F. & Souza Junior, J.A. 2010. Precipitação nas Mesorregiões do Estado do Pará: climatologia, variabilidade e tendências nas últimas décadas (1978–2008). *Revista Brasileira de Climatologia*, 6: 151-168.
- Almeida, L., Masselink, G., Russell, P. & Davidson, M. 2015. Observations of gravel beach dynamics during high energy wave conditions using a laser scanner. *Geomorphology*, 228: 15-27.
- Alvarez-Ellacuria, A., Orfila, A., Olabarrieta, M., Medina, R., Vizoso, G. & Tintoré, J. 2010. A Nearshore Wave and Current Operational Forecasting System. *Journal of Coastal Research*, 26: 503-509.
- ANA. Agência Nacional das Águas. 2013. Sistema de monitoramento hidrológico. Available in: <<http://bancodedados.cptec.inpe.br>>. Access on: 3 jun. 2013.
- Anthony, E.J., Levoy, F. & Montfort, O. 2004. Morphodynamics of intertidal bars on a megatidal beach, Merlimont, Northern France. *Marine Geology*, 208: 73-100.
- Beach, R.A. & Sternberg, R.W. 1996. Suspended sediment transport in the surf zone: response to breaking waves. *Continental Shelf Research*, 16: 1989-2003.
- Brand, E., Montreuil, A.L., Houthuys, R. & Chen,

- M. 2020. Relating Hydrodynamic Forcing and Topographic Response for Tide-Dominated Sandy Beaches. *Journal of Marine Science and Engineering*, 8: 151.
- Bulgin, C.E., Merchant, C.J. & Ferreira, D. 2020. Tendências, variabilidade, and persistence of sea surface temperature anomalies. *Scientific Reports*, 10: 7986.
- Bosboom, J., Reniers, A. & Lujendijk, A. 2014. On the perception of morphodynamic model skill. *Coastal Engineering*, 94: 112-125.
- Cartier, A. & Héquette, A. 2015. Vertical distribution of longshore sediment transport on barred macrotidal beaches, northern France. *Continental Shelf Research*, 95: 1-16.
- Cavalcante, G.H., Feary, D.A. & Kjerfve, B. 2013. Effects of Tidal Range Variability and Local Morphology on Hydrodynamic Behavior and Salinity Structure in the Caeté River Estuary, North Brazil. *International Journal of Oceanography*, 2013: 1-10.
- Carvalho L.P.F. 2007. Estudo morfoestratigráfico e sedimentológico dos depósitos holocênicos da planície costeira de Maracanã – NE do Pará. Belém, 129 p. Dissertação de Mestrado, Programa de Pós-graduação em Geologia e Geoquímica, Instituto de Geociências, Universidade Federal do Pará.
- CPTEC. Centro de Previsão de Tempo e Estudos Climáticos. 2013. Instituto Nacional de Pesquisas Espaciais. Banco de dados meteorológico (Modelo WWATCH). Available in: <<http://bancodedados.cptec.inpe.br>>. Access on: 14 jan. 2013.
- CPTEC. Centro de Previsão de Tempo e Estudos Climáticos. 2014. Instituto Nacional de Pesquisas Espaciais. Banco de dados meteorológico (Estação Synop). Available in: <<http://bancodedados.cptec.inpe.br>>. Access on: 25 jul. 2014.
- Dashtgard, S.E., MacEachern, J.A., Frey, S.E. & Gingras, M.K. 2012. Tidal effects on the shoreface: Towards a conceptual framework. *Sediment Geology*, 279: 42-61.
- De Miranda, L.B., Andutta, F.P., Kjerfve, B. & Castro Filho, B.M. 2017. *Fundamentals of estuarine physical oceanography*, vol. 8. Singapura, Springer, 480p.
- DHN. Diretoria de Hidrografia e Navegação. 1962. *Cartas de correntes de maré – Rio Pará – de Salinópolis à Belém*. Rio de Janeiro, DHN.
- Emery, W.J. & Thomson, R.E. 2014. Data analysis methods in physical oceanography, 3 ed. New York, Pergamon Press, 728 p.
- Geyer, W.R., Beardsley, R.C., Lentz, S.J., Candela, J., Limeburner, R., Johns, W.E., Castro, B.M. & Soares, I.D. 1996. Physical oceanography of the Amazon shelf. *Continental Shelf Research*, 16: 575-616.
- Holthuijsen, L.H. 2007. Waves in oceanic and coastal waters. Cambridge, Cambridge University Press, 404.
- Guo, L., Wang, Z.B., Townend, I. & Qing, H. 2019. Quantification of Tidal Asymmetry and Its Nonstationary Variations. *Journal of Geophysical Research*, 124: 773-787.
- Jamal, M.H., Simmonds, D. & Magar, V. 2014. Modelling gravel beach dynamics with XBeach. *Coastal Engineering* 89: 20-29.
- Kjerfve, B. 1989. Estuarine geomorphology and physical oceanography. In: Day, J.W., Hall, C.A.S., Kemp, W.M., Yañes-Arancibia, A. (Eds) Estuarine Ecology. New York, John, Wiley & Sons, pp 47-78.
- Levoy, F., Anthony, E.J., Monfort, O. & Larssonneur, C. 2000. Themorphodynamics of megatidal beaches in Normandy, France. *Marine Geology*, 171: 39-59.
- Masselink, G., Anthony, E.J. 2001. Location and height of intertidal bars on macrotidal ridge and runnel beaches. *Earth Surface Processes and Landforms*, 26: 759-774.
- Nascimento, A.T. & Pereira, L.C.C. 2016. Morphodynamic Processes on a Macrotidal Beach in the Eastern Amazon. *Journal of Coastal Research*, SI 75: 427-431.
- Ogton, A.S. & Sternberg, R.W. 2002. Effect of wave breaking on sediment eddy diffusivity, suspended-sediment and longshore sediment flux profiles in the surf zone. *Continental Shelf Research*, 40: 599-622.
- Oliveira, S.M.O., Pereira, L.C.C. & Vila-Concejo, A. 2014. Morphodynamic processes in a macrotidal beach in the Amazon littoral. *Quaternary and Environmental Geosciences*, 5: 125-136.
- Osborne, P.D. & Greenwood, B. 1993. Sediment suspension under waves and currents, time

- scales and vertical structures. *Sedimentology*, 40: 599-622.
- Owen, A. 2020. Tidal Current Energy: Origins and Challenge. In: Letcher, T.M. (Ed) Future Energy, 3rd ed. Amsterdam, Elsevier, pp. 357-374.
- Pereira, L.C.C., Silva, N.I.S., Costa, R.M., Asp, N.E., Costa, K. G. & Vila-Concejo, A. 2012. Seasonal changes in oceanographic processes at an equatorial macrotidal beach in northern Brazil. *Continental Shelf Research*, 43: 95-106.
- Pereira, L.C.C., Vila-Concejo, A. & Short, A.D. 2013. Influence of subtidal sand banks on tidal modulation of waves and beach morphology in Amazon macrotidal beaches. *Journal of Coastal Research*, SI 65: 1821-1826.
- Pereira, L.C.C., Vila-Concejo, A., Costa, R.M. & Short, A.D. 2014. Managing physical and anthropogenic hazards on macrotidal Amazon beaches. *Ocean and Coast Management*, 96: 149-162.
- Poate, T., Masselink, G., Davidson, M., McCall, R., Russell, P. & Turner, I. 2013. High frequency in-situ field measurements of morphological response on a fine gravel beach during energetic wave conditions. *Marine Geology*, 342: 1-13.
- Poate, T., Masselink, G., McCall, R., Russell, P. & Davidson, M. 2014. Storm-driven cusp behaviour on a high energy gravel beach. *Journal of Coastal Research*, SI 70: 645- 650.
- Prestes, Y.O., Silva, A.C., Rollnic, M. & Rosário, R.P. 2017. The M2 and M4 Tides in the Pará River Estuary. *Tropical Oceanography*, 45: 26-37.
- Ranieri, L.A. & El-Robrini, M. 2012. Avaliação experimental de métodos de armadilhas de sedimentos para determinação do transporte costeiro da Praia da Romana, Ilha dos Guarás (Nordeste do Pará). *Geociências*, 31: 103-116.
- Ranieri, L.A. & El-Robrini, M. 2015. Evolução da linha de costa de Salinópolis, Nordeste do Pará, Brasil. *Pesquisas em Geociências*, 42: 207-226.
- Ranieri, L.A. & El-Robrini, M. 2016. Quantificação de sedimentos transportados por correntes nas praias oceânicas de Salinópolis, Nordeste do Pará, Brasil. *Geociências*, 35: 457-471.
- Ranieri, L.A. & El-Robrini, M. 2020. Morfologia e Sedimentação em Praias Oceânicas da Amazônia Oriental durante a Variação Anual de Chuvas. *Revista Brasileira de Geografia Física*, 13(5): 2086-2102.
- Reichmüth, B. & Anthony, E.J. 2008. Seasonal-scale morphological and dynamic characteristics of multiple intertidal bars. *Zeitschrift für Geomorphology*, 52: 79-90
- Sá, J.H.S. 1969. Contribuição a geologia dos sedimentos Terciários e Quaternários da Região Bragantina. *Boletim do Instituto de Geologia*, 3:21-36.
- Sénéchal, N., Gouriou, T.B., Castelle, J., Parisot, S., Capo, S., Bujan, S. & Howa, H. 2009. Morphodynamic response of a meso- to macro-tidal intermediate beach based on a long-term data set. *Geomorphology*, 107: 263-274.
- Siegle, E.; Schettini, C.A.F., Klein, A.H.F. & Toldo Jr, E.E. 2009. Hydrodynamics and suspended sediment transport in the Camboriú Estuary - Brazil: pre jetty conditions. *Brazilian Journal of Oceanography*, 57: 123-135.
- Sipka, V. & Anthony, E.J. 1999. Morphology and hydrodynamics of a macrotidal ridge and runnel beach under modal low conditions. *Journal de Recherche Océanographique*, 24: 25-31.
- Souza Filho, P.W.M. & Paradella, W.R. 2003. Use of synthetic aperture radar for recognition of Coastal Geomorphological Features, land-use assessment and shoreline changes in Bragança coast, Pará, Northern Brazil. *Anais da Academia Brasileira de Ciências*, 75: 341-356.
- Torres, R., Uncles, R.J. 2011. Modeling of Estuarine and Coastal Waters. In: Wolanski, E. & Donald, M. (Eds) Treatise on Estuarine and Coastal Science. Academic Press, pp. 395-427.
- Utida, G., Cruz, F.W., Etourneau, J., Bouloubassi, J., Schefuß, E., Vuille, M., Novello, V.F., Prado, L.F., Sifeddine, A., Klein, V., Zular, A., Viana, J.C.C. & Turcq, B. 2019. Tropical South Atlantic influence on Northeastern Brazil precipitation and ITCZ displacement during the past 2300 years. *Scientific Reports*, 9: 1698.
- Vincent, C.E. & Osborne, P.D. 1995. Predicting suspended sand concentration profiles on a macrotidal beach. *Continental Shelf Research*, 15: 1497-1514.
- Voulgaris, G., Simmonds, D., Michel, D., Howa,

- H., Collins, M.B. & Huntley, D.A., 1998. Measuring and modelling sediment transport on a macrotidal ridge and runnel beach: an intercomparison. *Journal of Coastal Research*, 14: 315-330.
- Voulgaris, G. & Collins, M.B. 2000. Sediment resuspension on beaches: response to breaking waves. *Marine Geology*, 167: 167-187.
- Welch, P. 1967. The use of fast Fourier transform for the estimation of Power spectra: A method based on time averaging over short, modified periodograms. *IEEE Transactions on Audio and Electroacoustics*, 15: 70-73.
- White, T.E. 1998. Status of measurement techniques for coastal sediment transport. *Coastal Engineering*, 35: 17-45.
- Williams, L.L. & Lück-Vogel, M. 2020. Comparative assessment of the GIS based bathtub model and an enhanced bathtub model for coastal inundation. *Journal of Coastal Conservation*, 24: 23.
- Yu, Y., Sternberg, R.W. & Beach, R.A. 1993. Kinematics of breaking waves and associated suspended sediment in the nearshore zone. *Continental Shelf Research*, 13: 1219-1242.